Journal of Solid State Chemistry 184 (2011) 1649–1654

Contents lists available at ScienceDirect

Journal of Solid State Chemistry

journal homepage: www.elsevier.com/locate/jssc

Electronic structure of lanthanum copper oxychalcogenides LaCuO*Ch* (*Ch*=S, Se, Te) by X-ray photoelectron and absorption spectroscopy

Brent W. Rudyk, Peter E.R. Blanchard, Ronald G. Cavell, Arthur Mar*

Department of Chemistry, University of Alberta, Edmonton, Alberta, Canada T6G 2G2

ARTICLE INFO

Article history:
Received 8 March 2011
Received in revised form
24 April 2011
Accepted 2 May 2011
Available online 7 May 2011

Keywords:
Oxychalcogenides
XPS
XANES

ABSTRACT

X-ray photoelectron spectroscopy (XPS) and X-ray absorption near-edge spectroscopy (XANES) have been applied to examine the electronic structures of lanthanum copper oxychalcogenides LaCuO*Ch* (*Ch*=S, Se, Te), whose structure has been conventionally viewed as consisting of nominally isolated [LaO] and [Cu*Ch*] layers. However, there is evidence for weak La–*Ch* interactions between these layers, as seen in small changes in the satellite intensity of the La 3*d* XPS spectra as the chalcogen is changed and as supported by band structure calculations. The O 1*s* and Cu 2*p* XPS spectra are insensitive to chalcogen substitution. Lineshapes in the Cu 2*p* XPS spectra and fine-structure in the Cu L- and M-edge XANES spectra support the presence of Cu^{+} species. The *Ch* XPS spectra show negative BE shifts relative to the elemental chalcogen, indicative of anionic species; these shifts correlate well with greater difference in electronegativity between the Cu and *Ch* atoms, provided that an intermediate electronegativity is chosen for Se.

1. Introduction

Most representatives of the tetragonal ZrCuSiAs-type structure fall into two categories [1,2]: (i) rare-earth transition-metal oxypnictides *REMPn*O (*Pn*=P, As), which are now zealously investigated as new superconductors [3–7], and (ii) rare-earth copper oxychalcogenides *RE*CuO*Ch* (*Ch*=S, Se, Te), which have been identified as transparent p-type semiconductors [8–15]. (We follow the most common ways that these formulas have been written in the literature, even though the rules for element ordering are inconsistent.) In both cases, the physical properties derive from the partitioning of this structure into conducting [*MPn*] or [Cu*Ch*] layers interleaved with insulating [*RE*O] layers, a configuration that has been aptly described as a "multiple quantum well" (Fig. 1) [13]. The electronic interplay between the alternately stacked layers presents attractive opportunities to modify properties, such as the magnitude of the band gap in the oxychalcogenides, through appropriate chemical substitutions. Interestingly, the markedly two-dimensional character of the oxypnictides and oxychalcogenides does not extend to the eponymous compound ZrCuSiAs itself (as well as ZrCuSiP and HfCuSiAs), which exhibits strongly three-dimensional character as covalent Zr–As bonds form between the nominal [ZrSi] and [CuAs] layers [16,17].

We have previously applied X-ray photoelectron spectroscopy (XPS) and X-ray absorption near-edge spectroscopy (XANES) to monitor the changes in electronic structure upon chemical substitution in *REM*AsO and ZrCuSi*Pn* [18–20]. The small shifts in binding energy (BE) and absorption-edge energy in highly covalent systems such as these can now be routinely detected through the improved resolution available in modern XPS instrumentation and through the high source intensity associated with use of synchrotron radiation. From these studies, we have been able to correlate, for example, trends in the As BE with the difference in electronegativity in *M*–As bonds as *M* is altered in *REM*AsO, and trends in the Zr absorption-edge energy with the Zr-to-*Pn* charge transfer as *Pn* is altered in ZrCuSi*Pn*. In continuation of these studies on the electronic structure of ZrCuSiAs-type compounds, we present here an analysis of the high-resolution XPS core-line spectra and Cu absorption-edge spectra of LaCuO*Ch* (*Ch*=S, Se, Te). These results complement previous measurements of the valence and conduction band spectra of LaCuO*Ch*, obtained by Ueda and co-workers through photoemission and inverse photoemission spectroscopy [9,10,21], and of the *RE* 4*f* and O 2*p* partial densities of states of *RE*CuOS, obtained by Sato et al. [22] through resonant photoemission spectroscopy. In particular, the questions that we wish to address include how substitution of *Ch* affects the electronic structure in LaCuO*Ch* and how the BE shifts of the *Ch* atoms relate to the degree of electron transfer experienced within the [Cu*Ch*] layers.

2. Experimental

2.1. Synthesis

Reagents in the form of pieces (La) or powders (La_2O_3, Cu, S, Se, Te) with purities of 99.5% or better were obtained from Cerac, Aldrich, or Alfa-Aesar. For LaCuOS and LaCuOTe, mixtures of La,

* Corresponding author. Fax: +1 780 492 8231.
E-mail address: arthur.mar@ualberta.ca (A. Mar).

0022-4596/$ - see front matter © 2011 Elsevier Inc. All rights reserved.
doi:10.1016/j.jssc.2011.05.005

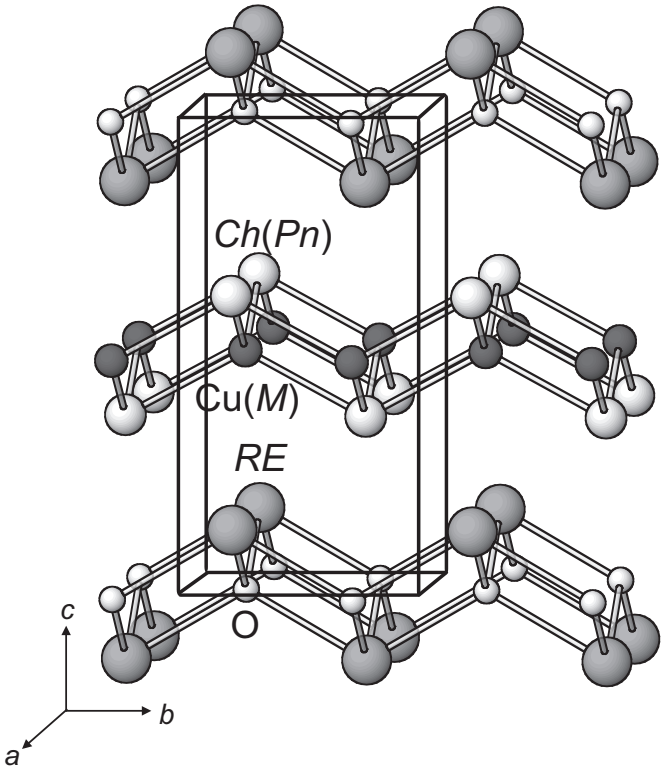

Fig. 1. Crystal structure of *RE*CuO*Ch* (*Ch*=S, Se, Te) (or *REMPn*O (*Pn*=P, As)) in terms of alternating [*REO*] and [Cu*Ch*] (or [*MPn*]) layers stacked along the *c*-direction.

La_2O_3, Cu, and *Ch* in a 1:1:3:3 ratio were placed in evacuated fused-silica tubes, which were sealed and heated at 1050 °C for 1–2 weeks, followed by quenching in water. Minor amounts of other phases, such La_2O_2S or La_2O_2Te, were detected after this initial heat treatment, presumably because of incomplete reaction, but they were readily eliminated after regrinding and reheating for an additional week. For LaCuOSe, this procedure could not lead to a sufficiently pure product to our satisfaction; instead, a more effective procedure was to react a mixture of La_2O_3, La_2Se_3 (prepared from stoichiometric reaction of La and Se at 900 °C for 1 week), Cu, and Se in a 2:1:6:3 ratio at 1050 °C for 10 d. All samples used for the spectroscopy measurements were phase-pure according to their powder X-ray diffraction patterns, collected on an Inel powder diffractometer (Fig. S1 in the Supplementary Data).

2.2. XPS analysis

XPS spectra were measured on a Kratos AXIS 165 spectrometer equipped with a monochromatic Al *K*α X-ray source (14 mA, 15 kV) and a hybrid lens with a spot size of $700 \times 400\ \mu m^2$. The air-stable samples were finely ground, pressed into In foil, mounted on a Cu sample holder with carbon tape, and transferred in a sealed container to the analysis chamber of the spectrometer. The pressure inside the XPS instrument was maintained between 10^{-7} and 10^{-9} Pa. Samples were sputter-cleaned with an Ar^+ ion beam (4 kV, 10 mA) until no further changes were observed in the peak shoulders associated with surface oxides, which could not be completely removed. Core-line BEs were, within standard uncertainties, the same before and after the sputtering procedure. Survey spectra (collected with a pass energy of 160 eV, step size of 0.7 eV, and sweep time of 180 s) in the range of 0–1100 eV confirmed the presence of all elements in the expected compositions. High-resolution spectra (collected with pass energy of 20 eV, step size of 0.05 eV, and sweep time of 180 s) were measured in the appropriate BE ranges as determined from the survey scan for the La 3*d*, Cu 2*p*, O 1*s*, and chalcogen (S 2*p*; Se 3*s*, 3*p*, 3*d*; Te 3*p*, 3*d*, 4*d*) core lines. Additional core-line spectra were measured for elemental Se and Te chosen as standards. Charge neutralization was determined to be unnecessary. The spectra were calibrated to the C 1*s* line at 284.8 eV arising from adventitious carbon and were analyzed with the use of the CasaXPS software package [23]. The background arising from energy loss was removed by applying a Shirley-type function and the peaks were fitted to pseudo-Voigt (70% Gaussian and 30% Lorentzian) line profiles to take into account spectrometer and lifetime broadening effects. On the basis of many previous measurements on this instrument, we estimate a precision of better than ± 0.1 eV in the BEs.

2.3. Cu XANES analysis

Cu L-edge spectra were measured on the high-resolution spherical grating monochromator undulator beamline (SGM, 11ID-1) and Cu M-edge spectra were measured on the variable line spacing plane grating monochromator beamline (VLS PGM, 11ID-2), both at the Canadian Light Source (CLS) in Saskatoon, Saskatchewan. Finely ground samples were mounted in a thin layer on carbon tape to the sample holder and inserted into the vacuum chamber via a load lock. Spectra were collected from ~15 eV below to ~30–40 eV above the edge to allow for normalization. For the Cu L-edge spectra, the step sizes were 0.5 eV in the pre- and post-edge regions and 0.1 eV through the edge; for the Cu M-edge spectra, the step sizes were decreased to 0.2 eV in the pre- and post-edge regions and 0.05 eV through the edge because of the lower X-ray intensity available in the PGM beamline. Although both total electron yield (TEY) and X-ray fluorescence yield (FLY) modes were used, we present only the FLY spectra because they suffer less from surface effects and are more intense than the TEY spectra. With the use of the program Hephaestus, these spectra were calibrated to Cu metal, with the maxima in the first derivatives set to 932.7 eV (L_3-edge) and 75.1 eV (M_3-edge); these spectra were analyzed with the use of the program Athena in the Ifeffit software package [24]. On the basis of previous measurements, we estimate a precision of ± 0.1 eV for the absorption edge energies.

2.4. Band structure calculations

Although tight-binding linear muffin tin orbital (TB-LMTO) band structure calculations have been previously conducted on LaCuO*Ch* (*Ch*=S, Se, Te), the crystal orbital Hamilton populations (COHP) were not reported [25]. We have repeated these calculations, with integrations carried out over 84 independent *k* points in the first Brillouin zone, to permit comparisons of integrated COHP values (–ICOHP) to LaNiAsO and ZrCuSiAs (Table S1 in the Supplementary Data) [26]. The density of states (DOS) and crystal orbital Hamilton population (COHP) curves are provided in Fig. S2 in the Supplementary Data.

3. Results and discussion

3.1. [LaO] layer

The La 3*d* spectra are similar for all members of LaCuO*Ch* (*Ch*=S, Se, Te), with essentially identical BEs of 834.3 eV for the $3d_{5/2}$ core line (Fig. 2) and 851.1 eV for the $3d_{3/2}$ core line (not shown). Although the La $3d_{5/2}$ BE is higher than in La_2O_3 (831.9 eV) and close to those in La*M*AsO (*M*=Fe, Co, Ni; 834.8 eV) [18], BE shifts of lanthanide atoms are not straightforward to interpret because they are quite sensitive to final-state

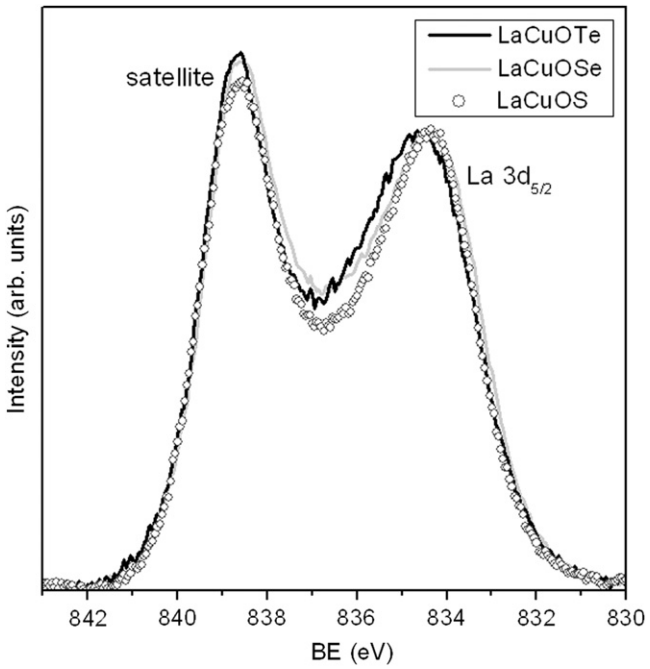

Fig. 2. La $3d_{5/2}$ XPS spectra for LaCuO*Ch* (*Ch*=S, Se, Te) normalized to the core-line peak to highlight intensity changes in the satellite peak.

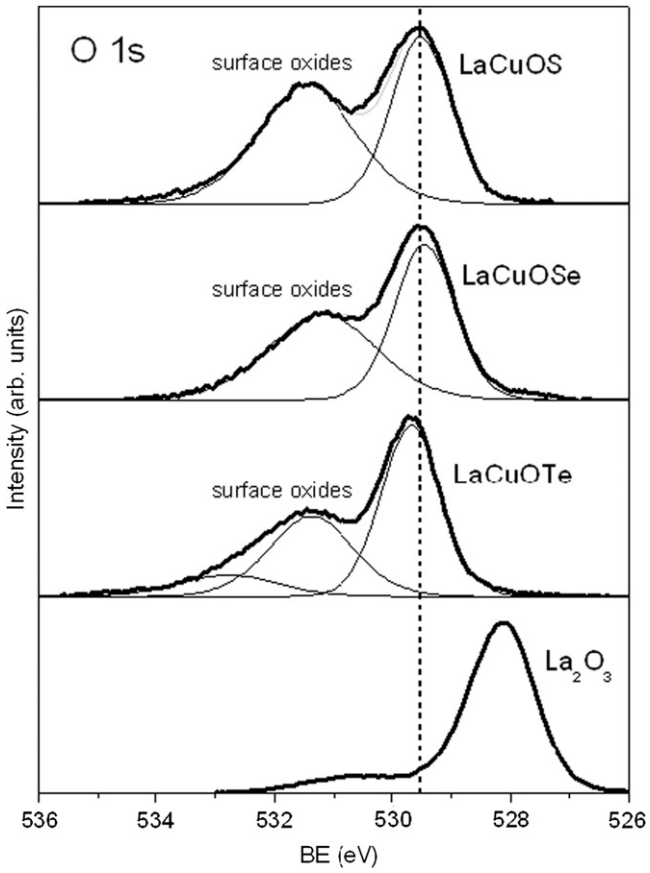

Fig. 3. Comparison of O 1*s* XPS spectra for LaCuO*Ch* (*Ch*=S, Se, Te), with the BE of 529.5–529.7 eV marked by the dashed vertical line, and La_2O_3.

effects and coordination environments [27–29]. The appearance of satellite peaks at 4 eV to the higher energy side of each of the core-line peaks is a diagnostic feature for La^{3+} species coordinated by other ligands (in contrast to the spectrum of La metal, which lacks these satellites) and is generally attributed to a ligand-to-metal shake-up process [30–32]. (Similar satellites are found in La_2O_3 [18], but for the same reasons as above, i.e. different coordination environments and final state effects, they cannot be directly compared to those found in LaCuO*Ch*.) When an electron is ejected after photoexcitation takes place, ligand-based valence electrons are promoted into La-based conduction states that are drawn lower in energy (below the Fermi level) by the core-hole. Although these satellites, induced by final-state effects, might be considered a nuisance, they do provide useful information. Their relative intensities depend on the degree of overlap between orbitals on the metal (La) and ligand atoms (O and *Ch*, at distances of 2.36–2.40 and 3.26–3.49 Å, respectively) [27–29]. When the spectra for LaCuO*Ch* are normalized to the La $3d_{5/2}$ core-line peak, the satellite peak becomes slightly more intense on progressing from LaCuOS to LaCuOSe and LaCuOTe (Fig. 2). Given that the O 1*s* spectra are invariant in this series (as presented shortly below), the change in the satellite intensity may be attributed to weak interactions of the La atoms in the [LaO] layer with more distant *Ch* atoms in the adjacent [Cu*Ch*] layer. The trend suggests that orbital overlap is more effective between La atoms and larger *Ch* atoms. LMTO calculations support this proposal, as seen in –ICOHP values for the La–*Ch* contacts of 0.11 eV/bond (3.26 Å) in LaCuOS, 0.13 eV/bond (3.33 Å) in LaCuOSe, and 0.17 eV bond (3.48 Å) in LaCuOTe. Of the competing factors that affect the degree of orbital overlap, the better matching of size and energy between La and larger *Ch* atoms overcomes their greater separation. The enhanced screening brought on by this more effective orbital overlap favours the promotion of *Ch*-based valence electrons to La-based conduction states in the ligand-to-metal shake-up process, increasing the cross-section and thus the intensity of the satellite peak [33,34].

The O 1*s* spectra have similar lineshapes and BEs in LaCuO*Ch* (Fig. 3). (The Ar^+ sputtering procedure reduced but could not remove all the surface oxides responsible for the peaks at higher BE; it did not affect the position and the lineshape of the core-line peaks, which have a FWHM of 1.2–1.3 eV.) The O 1*s* BEs (529.5 eV for LaCuOS and LaCuOSe; 529.7 eV for LaCuOTe) are higher than in La_2O_3 (528.8 eV) [27], but slightly lower than in La*M*AsO (529.9 eV) [18], indicating that the degree of ionic character in the La–O bonds in LaCuO*Ch* is intermediate between "very ionic" in La_2O_3 and "normal ionic" in La*M*AsO, if Barr's classification scheme is accepted [35,36]. The combined analysis of the La 3*d* and O 1*s* spectra provides evidence that weak La–*Ch* interactions exist between the nominally isolated [LaO] and [Cu*Ch*] layers, but they have little influence on the O atoms.

3.2. [CuCh] layer

Although the [Cu*Ch*] layer may be expected to be more sensitive to changes in *Ch*, the Cu 2*p* spectra are essentially identical for all members of the LaCuO*Ch* series (Fig. 4). No significant shifts are observed in the Cu $2p_{3/2}$ core-line peaks, for which the BEs of 932.7–932.9 eV are typical for Cu^{1+} and are lower than for most Cu^{2+} systems ($>$933.5 eV) [37–39]. However, the Cu $2p_{3/2}$ BE is not a reliable diagnostic for the Cu oxidation state; there are many compounds that cannot be distinguished this way (e.g., CuS and Cu_2S have identical BEs) [40], and in fact, Cu metal has a similar BE of 932.7 eV [41]. Stronger evidence for the presence of Cu^+ is gained from the FWHM of 1.0–1.2 eV (similar to that in CuBr and CuI [42,43], but smaller than $\sim$3 eV in CuO [39]) and the absence of a shake-up or shake-down satellite peak at the high-energy side of the $2p_{3/2}$ core-line that is characteristic of Cu^{2+} systems [44–47], as seen in CuO, for example (Fig. 4). The symmetrical lineshape of the Cu

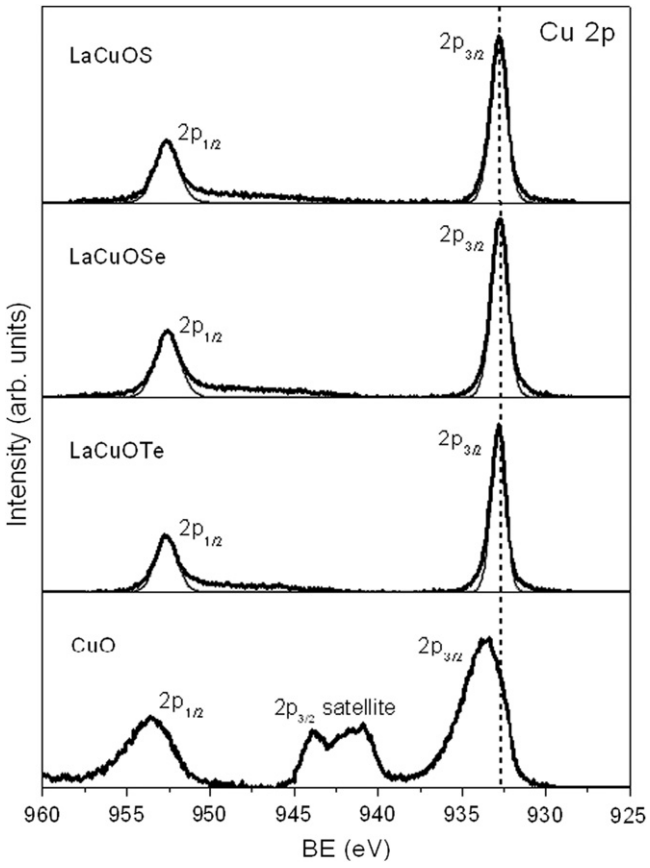

Fig. 4. Cu 2*p* XPS spectra for LaCuO*Ch* (*Ch*=S, Se, Te), with the $2p_{3/2}$ BE of 932.7–932.9 eV marked by the dashed vertical line. The spectrum for CuO is included to highlight the satellite peaks that would be characteristic for Cu^{2+} species.

$2p_{3/2}$ core-line peaks is consistent with the semiconducting behavior of these compounds. It has also been well-established that examination of the absolute shifts in the Cu $L_3M_{4,5}M_{4,5}$ Auger peak as well as the relative differences between this peak and the Cu $2p_{3/2}$ peak provides a reliable method to distinguish between Cu^{1+} and Cu^0 [48,49]. This Auger peak is shifted to slightly higher BE, by ~0.4 eV, in LaCuOSe relative to that in Cu metal (Fig. S3 in the Supplementary Data), consistent with the assignment of Cu^{1+}.

Further support for Cu^{1+} comes from analysis of the Cu XANES spectra (Fig. 5). In accordance with the selection rule $\Delta l = \pm 1$, the Cu L-edge spectra reveal transitions of electrons from the spin–orbit-split $2p_{3/2}$ (L_3-edge) or $2p_{1/2}$ (L_2-edge) states to available 3*d* (in the case of Cu^{2+}) or, with lower probability, 4*s* states (in the case of Cu^{1+} or Cu^0) [50]. Consistent with the assignment of Cu^{1+}, the absorption edges in LaCuO*Ch* show significant fine structure that originates from multiple excitations because the 4*s* states are hybridized with other states, and the L_3-edge energy (934.7–934.9 eV) is higher than in Cu metal (932.7 eV) [20,50]. Similarly, the Cu M-edge spectra reveal transitions from the spin–orbit-split $3p_{3/2}$ (M_3-edge) or $3p_{1/2}$ (M_2-edge) states to 3*d* or 4*s* states. These spectra are less intense and show the presence of surface oxides, but it is clear that the absorption edges in LaCuO*Ch* also shift to higher energies, relative to CuO and Cu metal standards.

The *Ch* XPS spectra reveal shifts to lower BEs for all core-line peaks relative to the element, indicative of anionic species (Fig. S4 in the Supplementary Data, with selected spectra in Fig. 6; BEs for the elements are averaged values taken from the NIST database [51]). The magnitude of these negative BE shifts follows a clear trend of 0.6–0.8 eV in LaCuOTe, 1.3–1.4 eV in LaCuOSe, and 2.2 eV

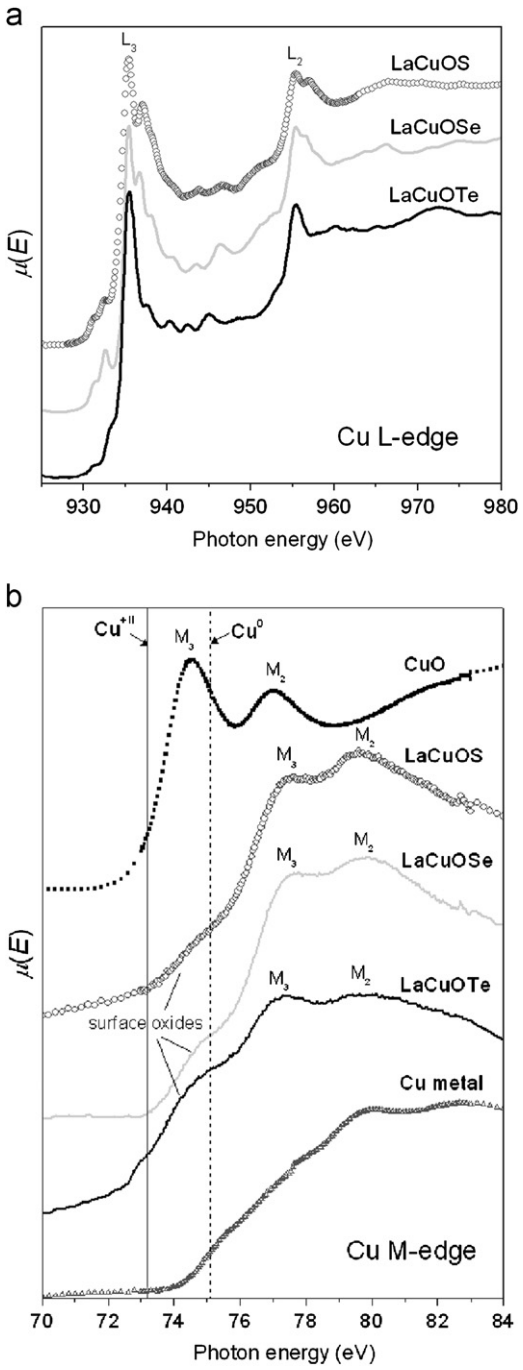

Fig. 5. (a) Cu L-edge and (b) Cu M-edge XANES spectra for LaCuO*Ch* (*Ch*=S, Se, Te), both measured in transmission mode. The spectra are offset for clarity. In (b), additional Cu M-edge spectra for CuO (with absorption edge at 73.2 eV marked by the solid vertical line) and Cu metal (with absorption edge at 75.1 eV marked by the dashed vertical line) are shown.

in LaCuOS. Because the *Ch* atoms are in identical environments in all compounds, the dominant effect must be a ground-state, intra-atomic one in which there is an inherent difference in their charge. The BE shifts may be expected to be more pronounced as the electron transfer from Cu to *Ch* atoms (in the Cu–*Ch* bonds) is enhanced with greater electronegativity of the *Ch* atom. However, conventional electronegativity definitions tend to place Se much closer to S than Te, as in the Pauling scale (S, 2.58; Se, 2.55; Te, 2.10) [52,53], or even in a reversed order, as in the Allred–Rochow scale (S, 2.44; Se, 2.48; Te, 2.01) [54]. A sensible correlation between the BE shift and the difference in electronegativity

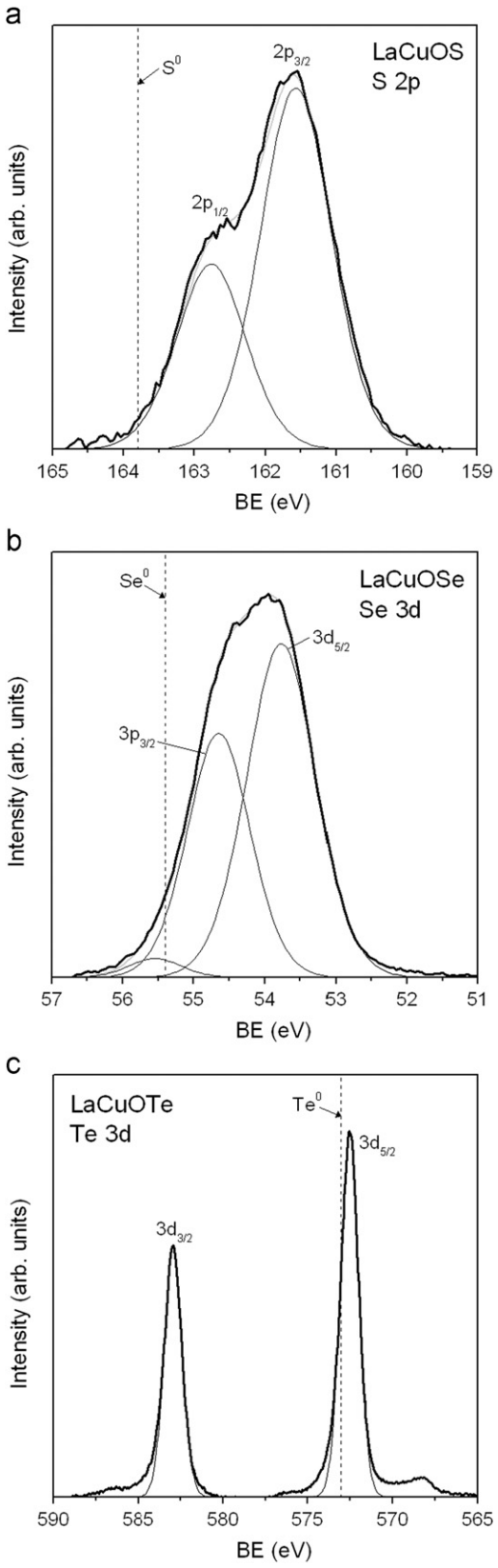

Fig. 6. Selected *Ch* core-line XPS spectra for LaCuO*Ch* (*Ch*=S, Se, Te). The BEs for the elemental chalcogens (163.8 eV for S $2p_{3/2}$; 55.4 eV for Se $3d_{5/2}$; 573.0 eV for Te $3d_{5/2}$) are marked by dashed vertical lines. (A small Cu LMM Auger peak appears at 567 eV in the spectrum for LaCuOTe.)

($\Delta\chi=\chi_{Ch}-\chi_{Cu}$) can be achieved only if an intermediate value is chosen for Se. In fact, if a corrected electronegativity for Se is taken simply as the average of that of S and Te in the Allred–Rochow scale,

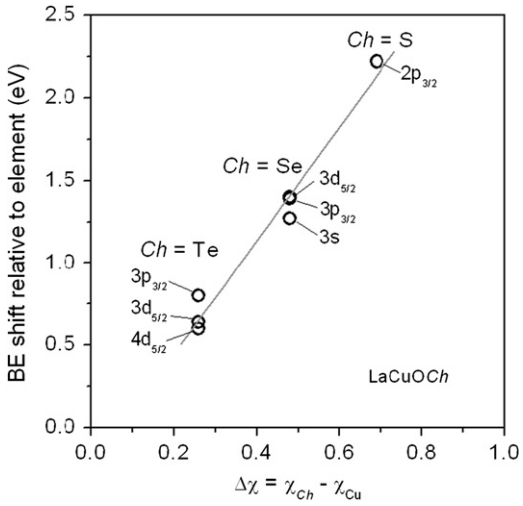

Fig. 7. Plot of *Ch* BE shifts (negative) for LaCuO*Ch* (*Ch*=S, Se, Te) relative to the elemental chalcogens vs. difference in electronegativity between *Ch* and Cu.

a plot of BE shift vs. $\Delta\chi$ is roughly linear (Fig. 7). This result lends merit to other scales that place Se at an intermediate value, such as the Allen scale, for which "spectroscopic electronegativities" are defined on the basis of average one-electron energies in a singly ionized atom [55]. For a given compound LaCuO*Ch*, peaks derived from deeper core levels tend to experience slightly greater BE shifts than those from shallower core levels (cf., 0.80 eV ($3p_{3/2}$), 0.64 eV ($3d_{5/2}$), 0.60 eV ($4d_{5/2}$) for the Te atoms in LaCuOTe).

3.3. Comparison with REMAsO and ZrCuSiAs

It is instructive to compare the XPS and XANES analyses for LaCuO*Ch* with the isostructural compounds *REM*AsO and ZrCuSi*Pn* [18–20]. The [LaO] layers common to both La*M*AsO and LaCuO*Ch* are essentially identical, as indicated by the similar BE shifts and lineshapes for the La and O core-line peaks. Within the [*M*As] layer of the La*M*AsO series, there are discernable shifts in the As BE, attributed to ground-state effects, as the *M*-to-As charge transfer is enhanced in the progression of *M* from Ni to Fe. Within the analogous [Cu*Ch*] layer of the LaCuO*Ch* series, it might be anticipated that corresponding shifts in the Cu XPS spectra would reflect the degree of Cu-to-*Ch* charge transfer as *Ch* is changed, but none is observed because of the insensitivity of the Cu $2p_{3/2}$ BE, probably because of final-state effects [56] facilitated, in part, by the presence of weak Cu–Cu bonding (2.8–3.0 Å). However, clear evidence for this charge transfer is provided by the *Ch* core-line peaks, which undergo negative BE shifts (relative to the elemental chalcogen) that become more pronounced with a greater difference in electronegativity ($\chi_{Ch}-\chi_{Cu}$). Both *REM*AsO and LaCuO*Ch* have been typically portrayed as highly two-dimensional structures consisting of independent [*RE*O] layers interleaved with [*M*As] or [Cu*Ch*] layers, respectively. In large measure, this is a reasonably accurate picture: analysis of –ICOHP values obtained from band structure calculations suggests that interlayer bonding accounts for only 4% of the (covalent) bonding energy in LaNiAsO (as evaluated from the La–As interactions of 3.4 Å between the [LaO] and [NiAs] layers) and between 4% and 6% in LaCuO*Ch* (as evaluated from the La–*Ch* interactions of 3.3–3.5 Å between the [LaO] and [Cu*Ch*] layers). Small differences in the satellite intensity of the La 3*d* XPS spectra in LaCuO*Ch* are suggestive of these weak La–*Ch* interactions. In contrast, ZrCuSi*Pn* exhibits three-dimensional bonding character in ZrCuSi*Pn* (e.g., interlayer Zr–As bonding between the nominal [ZrSi] and [CuAs] layers accounts for 26% of the covalent bonding energy in

ZrCuSiAs), which is manifested by significant shifts in the Zr K-edge absorption energy when *Pn* is changed from As to P.

The XPS analysis of the chalcogen and pnicogen atoms in these compounds deserves further comment. Although they are not yet well-systematized, core-line BE shifts for the anionic species of the heavier *p*-block elements generally become less pronounced on proceeding from the chalcogens to the pnicogens, in accordance with expectations. These shifts correlate well with differences in electronegativity, provided that they are revised to more intermediate values for the fourth-period elements (Se, 2.22; As, 1.94) if the Allred–Rochow scale is chosen [57]. Thus, for example, the shifts in the Se core-line BEs are much larger in LaCuOSe (1.3–1.4 eV; $\chi_{Se}-\chi_{Cu}=2.22-1.75=0.47$) than in the As core-line BEs in LaNiAsO (0.3 eV; $\chi_{As}-\chi_{Ni}=1.94-1.75=0.19$) and ZrCuSiAs (0.6 eV; $\chi_{As}-\chi_{Cu}=1.94-1.75=0.19$) [18,20]. Because LaCuO*Ch* and La*M*AsO are isostructural, it would be interesting to attempt to prepare mixed-anion derivatives such as LaCuO(*Ch*, As), for which the properties could be tuned from a semiconductor to a metal through a change in the electron count. An understanding of these BE shifts will be useful in the eventual analysis of these more complicated systems.

Acknowledgments

This work was supported through Discovery Grants to A.M. and R.G.C. from the Natural Sciences and Engineering Research Council (NSERC) of Canada. Access to the Kratos AXIS 165 XPS spectrometer was provided by the Alberta Centre for Surface Engineering and Science (ACSES), which was established with support from the Canada Foundation for Innovation (CFI) and Alberta Innovation and Science. We thank Dr. T.K. Sham, Tom Regier, and David Chevrier for the assistance with the Cu L-edge XANES experiments on the SGM beamline, and Lucia Zuin for the assistance with the Cu M-edge XANES experiments on the VLS-PGM beamline at CLS, which are operated with support from NSERC, NRC, CIHR, and the University of Saskatchewan.

Appendix A. Supporting information

Supplementary data associated with this article can be found in the online version at doi:10.1016/j.jssc.2011.05.005.

References

[1] R. Pöttgen, D. Johrendt, Z. Naturforsch. B 63 (2008) 1135–1148.
[2] S.J. Clarke, P. Adamson, S.J.C. Herkelrath, O.J. Rutt, D.R. Parker, M.J. Pitcher, C.F. Smura, Inorg. Chem. 47 (2008) 8473–8486.
[3] B.I. Zimmer, W. Jeitschko, J.H. Albering, R. Glaum, M. Reehuis, J. Alloys Compd. 229 (1995) 238–242.
[4] P. Quebe, L.J. Terbüchte, W. Jeitschko, J. Alloys Compd. 302 (2000) 70–74.
[5] Y. Kamihara, H. Hiramatsu, M. Hirano, R. Kawamura, H. Yanagi, T. Kamiya, H. Hosono, J. Am. Chem. Soc. 128 (2006) 10012–10013.
[6] H. Takahashi, K. Igawa, K. Arii, Y. Kamihara, M. Hirano, H. Hosono, Nature 453 (2008) 376–378.
[7] Y.-W. Ma, Z.-S. Gao, L. Wang, Y.-P. Qi, D.-L. Wang, X.-P. Zhang, Chin. Phys. Lett 26 (2009) 037401-1–037401-4.
[8] M. Palazzi, C. Carcaly, J. Flahaut, J. Solid State Chem. 35 (1980) 150–155.
[9] S. Inoue, K. Ueda, H. Hosono, N. Hamada, Phys. Rev. B 64 (2001) 245211-1–245211-5.
[10] K. Ueda, K. Takafuji, H. Hiramatsu, H. Ohta, T. Kamiya, M. Hirano, H. Hosono, Chem. Mater. 15 (2003) 3692–3695.
[11] H. Hiramatsu, H. Kamioka, K. Ueda, M. Hirano, H. Hosono, J. Ceram. Soc. Jpn. 113 (2005) 10–16.
[12] H. Hiramatsu, K. Ueda, H. Ohta, T. Kamiya, M. Hirano, H. Hosono, Appl. Phys. Lett. 87 (2005) 211107-1–211107-3.
[13] K. Ueda, H. Hiramatsu, M. Hirano, T. Kamiya, H. Hosono, Thin Solid Films 496 (2006) 8–15.
[14] H. Hiramatsu, H. Kamioka, K. Ueda, H. Ohta, T. Kamiya, M. Hirano, H. Hosono, Phys. Status Solidi A 203 (2006) 2800–2811.
[15] H. Hiramatsu, H. Yanagi, T. Kamiya, K. Ueda, M. Hirano, H. Hosono, Chem. Mater. 20 (2008) 326–334.
[16] V. Johnson, W. Jeitschko, J. Solid State Chem. 11 (1974) 161–166.
[17] H. Abe, K. Yoshii, J. Solid State Chem. 165 (2002) 372–374.
[18] P.E.R. Blanchard, B.R. Slater, R.G. Cavell, A. Mar, A.P. Grosvenor, Solid State Sci. 12 (2010) 50–58.
[19] P.E.R. Blanchard, R.G. Cavell, A. Mar, J. Solid State Chem. 183 (2010) 1477–1483.
[20] P.E.R. Blanchard, R.G. Cavell, A. Mar, J. Solid State Chem. 183 (2010) 1536–1544.
[21] K. Ueda, H. Hosono, N. Hamada, J. Appl. Phys 98 (2005) 043506-1–043506-7.
[22] H. Sato, S. Nishimoto, K. Tsuji, K. Takase, H. Nakao, Y. Takahashi, T. Takano, K. Sekizawa, H. Negishi, S. Negishi, M. Nakatake, H. Namatame, M. Taniguchi, J. Alloys Compd. 408–412 (2006) 746–749.
[23] N. Fairley, CasaXPS, Version 2.3.9, Casa Software Ltd., Teighnmouth, Devon, UK, 2003.
[24] B. Ravel, M. Newville, J. Synchrotron Radiat. 12 (2005) 537–541.
[25] M.L. Liu, L.B. Wu, F.Q. Huang, L.D. Chen, J.A. Ibers, J. Solid State Chem. 180 (2007) 62–69.
[26] R. Tank, O. Jepsen, A. Burkhardt, O.K. Andersen, TB-LMTO-ASA Program, Version 4.7, Max Planck Institut für Festkörperforschung, Stuttgart, Germany, 1998.
[27] W. Grünert, U. Sauerlandt, R. Schlögl, H.G. Karge, J. Phys. Chem. 97 (1993) 1413–1419.
[28] E. Talik, A. Novosselov, M. Kulpa, A. Pajaczkowska, J. Alloys Compd. 321 (2001) 24–26.
[29] A. Novosselov, E. Talik, A. Pajaczkowska, J. Alloys Compd. 351 (2003) 50–53.
[30] A.J. Signorelli, R.G. Hayes, Phys. Rev. B 8 (1973) 81–86.
[31] G. Crecelius, G.K. Wertheim, D.N.E. Buchanan, Phys. Rev. B 18 (1978) 6519–6524.
[32] S.-J. Oh, G.-H. Kim, G.A. Sawatzky, H.T. Jonkman, Phys. Rev. B 37 (1988) 6145–6152.
[33] J.H. Scofield, J. Electron Spectrosc. Relat. Phenom. 8 (1976) 129–137.
[34] J.J. Yeh, I. Lindau, At. Data Nucl. Data Tables 32 (1985) 1–155.
[35] T.L. Barr, Modern ESCA: The Principles and Practice of X-Ray Photoelectron Spectroscopy, CRC Press, Boca Raton, FL, 1994.
[36] V. Dimitrov, T. Komatsu, J. Solid State Chem. 163 (2002) 100–112.
[37] D.C. Frost, A. Ishitani, C.A. McDowell, Mol. Phys. 24 (1972) 861–877.
[38] R.P. Vasquez, Surf. Sci. Spectra 5 (1998) 257–261.
[39] R.P. Vasquez, Surf. Sci. Spectra 5 (1998) 262–266.
[40] S.K. Chawla, N. Sankarraman, J.H. Payer, J. Electron Spectrosc. Relat. Phenom. 61 (1992) 1–18.
[41] A.C. Miller, G.W. Simmons, Surf. Sci. Spectra 2 (1993) 55–60.
[42] R.P. Vasquez, Surf. Sci. Spectra 2 (1993) 144–148.
[43] R.P. Vasquez, Surf. Sci. Spectra 2 (1993) 149–154.
[44] A. Rosencwaig, G.K. Wertheim, J. Electron Spectrosc. Relat. Phenom. 1 (1972/73) 493–496.
[45] F. Werfel, M. Heinonen, E. Suoninen, Z. Phys. B: Condens. Matter 70 (1988) 317–322.
[46] A. Roberts, D. Engelberg, Y. Liu, G.E. Thompson, M.R. Alexander, Surf. Interface Anal. 33 (2002) 697–703.
[47] T. Ghodselahi, M.A. Vesaghi, A. Shafiekhani, A. Baghizadeh, M. Lameii, Appl. Surf. Sci. 255 (2008) 2730–2734.
[48] T.H. Fleisch, G.J. Mains, Appl. Surf. Sci. 10 (1992) 51–62.
[49] J.P. Espinós, J. Morales, A. Barranco, A. Caballero, J.P. Holgado, A.R. González-Elipe, J. Phys. Chem. B 106 (2002) 6921–6929.
[50] R.A.D. Pattrick, G. van der Laan, J.M. Charnock, B.A. Grguric, Am. Mineral. 89 (2004) 541–546.
[51] C.D. Wagner, A.V. Naumkin, A. Kraut-Vass, J.W. Allison, C.J. Powell, J.R. Rumble Jr., NIST X-ray Photoelectron Spectroscopy Database, Version 3.5 (web version), National Institute of Standards and Technology, Gaithersburg, MD, 2003.
[52] A.L. Allred, J. Inorg. Nucl. Chem. 17 (1961) 215–221.
[53] L.R. Murphy, T.L. Meek, A.L. Allred, L.C. Allen, J. Phys. Chem. A 104 (2000) 5867–5871.
[54] A.L. Allred, E.G. Rochow, J. Inorg. Nucl. Chem. 5 (1958) 264–268.
[55] L.C. Allen, J. Am. Chem. Soc. 111 (1989) 9003–9014.
[56] P.A.W. van der Heide, J. Electron Spectrosc. Relat. Phenom. 151 (2006) 79–91.
[57] A.P. Grosvenor, R.G. Cavell, A. Mar, J. Solid State Chem. 181 (2008) 2549–2558.